Periodica Polytechnica
Transportation Engineering

44(1), pp. 42-49, 2016
DOI: 10.3311/PPtr.8208

Hydroplaning on Sloping Pavements Based on Inertial Measurement Unit (IMU) and 1mm 3D Laser Imaging Data

Wenting Luo[1], Kelvin C. P. Wang[2*], Lin Li[1]

RESEARCH ARTICLE

Received 05 May 2015; accepted after revision 10 August 2015

Abstract

The hydroplaning risk would increase on sloping pavements due to the fact that the presence of longitudinal and cross slopes would decrease the wheel load of vehicles perpendicular to the pavement surface. In previous studies, the effects of pavement slope on vertical wheel load and relevant hydroplaning speed prediction are ignored. To address this potential problem, the paper presents two improved models based on the existing Gallaway and University of South Florida (USF) models. Firstly, 1mm 3D laser imaging data is continuously collected at highway speed with the 1mm 3D PaveVision3D Ultra system, and simultaneously cross slope is acquired with an Inertial Measurement Unit (IMU) system and calibrated with1mm 3D data. A 4.35 km pavement section with five horizontal curves is selected to investigate hydroplaning speed predicted from Gallawayand USF models, and the two improved models. 1mm 3D pavement surface data is used to estimate texture information for the models in lieu of traditional spot-laser based texture measurement devices. Findings show that hydroplaning speeds at pavement segments with large slopes are lower than that at pavement segments with no grades. Moreover, pavement segments with potential hydroplaning risk are identified by comparing predicted hydroplaning speeds with posted speed limit. The significance of this paper is integrating the real-time 1mm 3D texture data and IMU data into the improved models for potential hydroplaning prediction of sloping pavement in network level survey.

Keywords

Hydroplaning Speed, Sloping Pavement, Gallaway Model, University of South Florida (USF) Model, Inertial Measurement Unit (IMU), 3D Laser Imaging

[1] College of Transportation and Civil Engineering,
Fujian Agriculture Forestry University,
Fuzhou, Fujian Province, 350108, PR China

[2] School of Civil and Environmental Engineering,
Oklahoma State University, Stillwater OK, USA 74078,

* Corresponding author, e-mail: kelvin.wang@okstate.edu

1 Introduction

Pavement hydroplaning occurs when water pressures build up in front of a moving tire resulting in an uplift force sufficient to separate the tire from the pavement. The loss of steering and traction force produced during hydroplaning may cause the vehicle to lose control, especially when a steering tire is involved (Kumar et al., 2009). Past studies indicated the occurrence of hydroplaning is highly associated with several factors, including pavement texture, cross slope, longitudinal grade, pavement width, pavement types, pavement condition, tire characteristics, and rainfall intensity (Khedr and Breakah, 2011; Berta and Torok, 2009; Goyal, 2003).

Numerous field studies were dedicated to developing hydroplaning prediction models in the past decades (Horne and Dreher, 1963) and results of hydroplaning (Dabbour, 2012). The models can be grouped into two categories: empirical models and analytical models (Chesterton et al., 2006). The empirical methods use experimental data and equations to predict hydroplaning, including Road Research Laboratory (RRL) equations to estimate water film depth (WFD) (Russam and Ross, 1968), National Aeronautics and Space Administration (NASA) models developed based on aircraft tire and airport pavement data (Horne and Dreher, 1963), and Gallaway model to predict roadway hydroplaning (Gallaway et al., 1979). The analytical methods attempt to mathematically model hydroplaning of the sheet flow and its interaction with a tire, including PAVDRN computer program developed by Pennsylvania State University (Huebner et al., 1996), and the University of South Florida (USF) model based on Ong and Fwa's numerical prediction (Guaratne et al., 2012).

Pavement slope, also termed as flow path slope, consists of cross slope and longitudinal grade, which exerts a tremendous influence on hydroplaning prediction (Zhang et al., 2005). To maintain constant water film, hydroplaning simulation tests in past studies were conducted on straight and flat pavements (Gallaway and Rose, 1971; Ong and Fwa, 2007). For pavement segments with the horizontal curve and large longitudinal grade, a smaller uplift force of water can cause hydroplaning issues due to the reduced vertical wheel load caused by

large slopes. However, past studies on hydroplaning prediction neglected the influences of pavement slope on vertical wheel loads of vehicles. The existing hydroplaning prediction models overestimate hydroplaning speed, and particularly are not suitable to analyze pavements with large pavement slope.

The aims of this study include:

- properly predict hydroplaning speeds on pavement with large slopes using hydroplaning prediction model;
- calibrate the IMU measured cross slope by eliminating the effects of survey vehicle vibration;
- identify the potential hydroplaning segments in network level survey.

In order to achieve these aims, first, two improved models are presented in this study on the basis of the existing Gallaway and USF models, in which the effects of flow path slope on vertical wheel load are considered and the sensitivities of the variables to hydroplaning speed predictions are examined. In this study, the WayLink Digital Highway Data Vehicle (DHDV) with the new 1mm 3D PaveVision3D Ultra technology and an Inertial Measurement Unit (IMU) system is used to collect pavement surface data including 1mm 3D laser imaging data, cross slope, and longitudinal grade data. The 1mm 3D pavement surface data is directly used for estimating pavement macro-texture in lieu of using traditional spot-laser devices. Texture data is a key input for the presented hydroplaning models. A flexible pavement section with five horizontal curves is chosen as examples to investigate the potential hydroplaning risks of both straight roads and curved roads. Finally, based on the predicted hydroplaning speed and posted speed limit, pavement segments with potential hydroplaning risk can be identified for pavement engineers to take corrective measures such as constructing superior texture, posting proper speed traffic signs etc. to minimize potential traffic accidents caused by hydroplaning issues, and enhance pavement safety.

2 Prediction Models of Hydroplaning Speed

2.1 Gallaway and USF Models

The Gallaway model is an empirical method developed by Gallaway et al. (1979) for the US Department of Transportation. The method described in Eq. (1)-(5) was adopted in the Texas Department of Transportation Hydraulic Design Manual (Gallaway et al., 1979). The flow path, an important factor on hydroplaning prediction model, can be defined in Fig. 1 and calculated with Eq. (1). The USF model is an analytical hydroplaning prediction model developed at the University of South Florida based on Ong and Fwa's comprehensive numerical prediction, shown in Eq. (6). The USF model can be used to predict the hydroplaning speeds for different light vehicles that employ tires compatible with the locked-wheel tester tires (Guaratne et al., 2012).

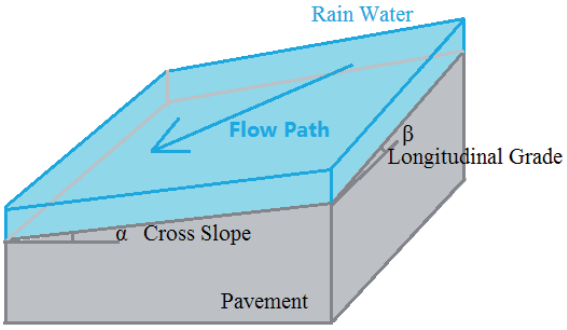

Fig. 1 Schematic diagram of cross slope, longitudinal grade, and flow path

$$S_f = \left(S_l^2 + S_c^2\right)^{1/2} \tag{1}$$

$$L_f = W_p \times \left(S_f / S_c\right) \tag{2}$$

$$WFD = 0.01485\left[\left(MTD^{0.11} \times L_f{}^{0.43} \times I^{0.59}\right) / \left(S_c{}^{0.42}\right)\right] - MTD \tag{3}$$

$$A = \text{Max. of} \begin{cases} \left(\dfrac{12.639}{WFD^{0.06}}\right) + 3.50 \\ \left[\left(\dfrac{22.351}{WFD^{0.06}}\right) - 4.97\right] \times MTD^{0.14} \end{cases} \tag{4}$$

$$v_p = 0.9143 \times SD^{0.04} \times P_t^{0.3} \times \left(TD + 0.794\right)^{0.06} \times A \tag{5}$$

$$v_p = W^{0.2} \times P_t^{0.5} \times \left[\left(\frac{0.82}{WFD^{0.06}}\right) + 0.49\right] \tag{6}$$

Where, WFD : Water film depth (mm); MTD : Meantexture depth (mm) calculated from the macro texture data; v_p : Hydroplaning speed (km/h); L_f : Pavement flow path length (m); S_c : Cross slope (m/m); S_l : Longitudinal grade (m/m); W_p : Pavement width (m); I : Rainfall intensity (mm/hr); P_t : Inflation pressure (Kpa); SD : Spin down ratio; TD : Tire tread depth (mm); W : Wheel load (N).

2.2 Effects of Pavement Slope on Vertical Wheel Load

Typically cross slope or longitudinal grade would reduce the vertical wheel load of vehicles on pavement surface (Shafabakhsh and Kashi, 2015). Hydroplaning occurs when the vertical wheel load is equivalent to the uplift force by water (Eq. (7)), and the steering and traction force would be lost during hydroplaning.

Figure 2 (a) shows the pavement section with a large longitudinal grade. When the vehicle travels on this pavement segment, the vehicle gravity center would be partitioned into two components of forces: one (wheel load) is perpendicular with

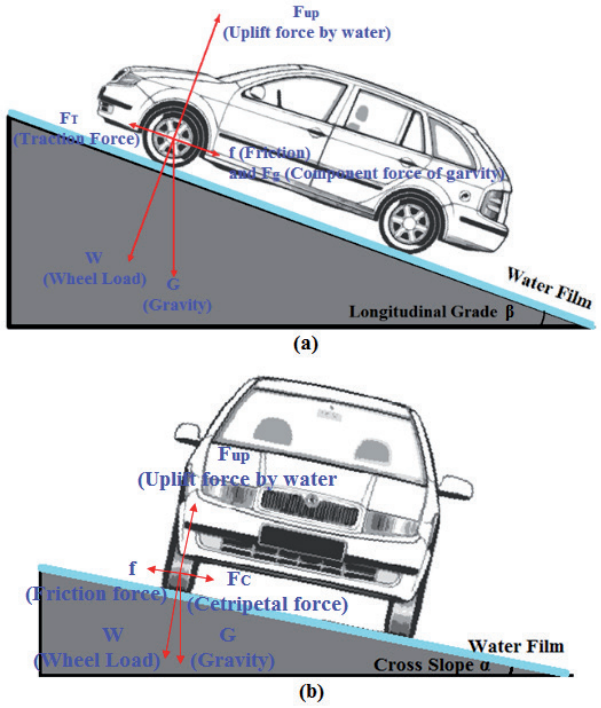

Fig. 2 Vehicle travelling on (a)pavements segments with longitudinal grade; (b) pavement segment with horizontal curve

the travelling surface, and the other one (traction force) is parallel with pavement surface. The wheel load would decrease with the increase of longitudinal grade (Eq. (8)), and the reduced wheel load would increase the hydroplaning risk.

Figure 2(b) shows the pavement section with horizontal curves or large cross slope. Similarly, the vehicle gravitycenter is partitioned into two components of forces when the vehicle travels on the horizontal curve. One component of force is the wheel load, and the other one is the centripetal force shown in Fig. 2(b). The wheel load on the horizontal curve would decrease with the increase of super-elevation (Eq. (9)). Finally, the wheel load can be calculated with flow path slope by combining the cross slope and longitudinal grade, as given in Eq. (10).

$$F_{Up} = W \tag{7}$$

$$W_L = G \times \cos(\beta) \tag{8}$$

$$W_C = G \times \cos(\alpha) \tag{9}$$

$$W = G \times \cos(\rho) \tag{10}$$

Where: F_{Up} : Minimum uplift force causing hydroplaning (N); W : Wheel load (N); W_L : Wheel load in longitudinal section (N); W_c : Wheel load in cross-section (N); G : Gravity of vehicle (N); β : Angle of longitudinal grade (degree); α : Angle of cross slope (degree); ρ : Angle of flow path slope (degree).

2.3 Improved Hydroplaning Speed Prediction Models

In the current models, the influences of flow path slope on vertical wheel load are not taken into account in hydroplaning prediction models. Therefore, this study aims at improving the existing Gallaway and USF models by considering the effects of flow path slope on wheel loads, as shown in Eqs. (11) and (12).

$$v_p = 0.9143 \times SD^{0.04} \times \left(P_t \times \cos\rho\right)^{0.3} \times (TD + 0.794)^{0.06} \times A \tag{11}$$

$$v_p = \left(W \times \cos\rho\right)^{0.2} \times \left(P_t \times \cos\rho\right)^{0.5} \times \left(0.82/WFD^{0.06} + 0.49\right) \tag{12}$$

Where: W : Wheel load (N); WFD : Water film depth (mm); P_t : Inflation pressure (Kpa); SD : Spin down ratio; TD : Tire tread depth (mm); A : Maximum value of Eq. (4); ρ : Angle of flow path slope (degree).

2.4 Sensitivity Analysis of the Improved Models

To explore the sensitivity of cross slope and longitudinal grade on hydroplaning speed, the cross slope and longitudinal grade change by ± 25%, ± 50%, and ± 75% individually while the other variables are maintained constant values. The constant values of each factor is assumed to be the average values of that factor measured for test site, as provided as follows:

- Cross slope: S_c = 1.53%
- Rainfall intensity: I = 148.4 *mm/hr*
- Mean texture depth: MTD = 1.2 mm
- Longitudinal grade: S_l =1.32%

The results of sensitivity analysis from the improved Gallaway and USF models to cross slope and longitudinal grade are given in Fig. 3. It can be seen that the resulting change in hydroplaning speed, "V_P", is apparent along the increase of cross slope and longitudinal grade. In the two improved models, the hydroplaning speed is affected by both the vertical load and the flow path length. Typically the increase in cross slope or longitudinal grade would diminish the vertical wheel load. The increase in cross slope would shorten the flow path length while the increase in longitudinal grades would extend the flow path length. Both the decrease in vertical load and the increase in flow path length would reduce the hydroplaning speed.

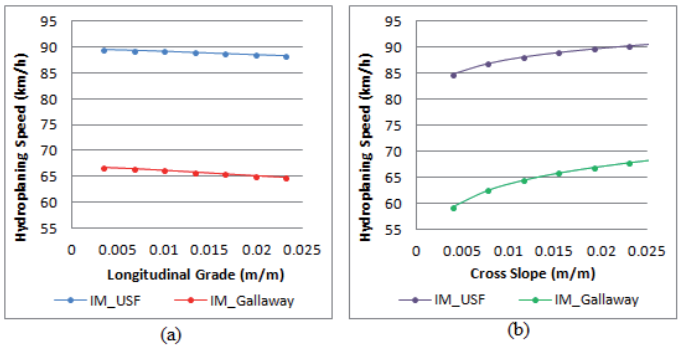

Fig. 3 Sensitivity test for two improved models: (a) longitudinal grade vs. hydroplaning speed; (b) cross slope vs. hydroplaning speed.

Accordingly the hydroplaning speed should decrease with the increase of longitudinal slope, and may either increase or decrease with the increase of cross slope depending on effects of vertical load and flow paths. Figure 3 shows that hydroplaning speed goes up with the increase of the cross slope, indicating the effect of flow path length on hydroplaning speed is greater than that of wheel load. It is shown that hydroplaning speed is more sensitive to the cross slope than longitudinal grade in the two improved models.

3 Data Acquisition Systems

3.1 Digital Highway Data Vehicle (DHDV) with PaveVision3D

DHDV, developed by the WayLink Systems Corporation with collaborations from the University of Arkansas and the Oklahoma State University, has evolved into a sophisticated system to conduct full lane data collection in 3D on roadways at highway speed up to 100 km/h. With the latest PaveVision3D Ultra (3D Ultra in short), the resolutions of surface 3D data are about 0.3 mm in vertical direction and 1 mm in the longitudinal and transverse directions, all achieved at 100km/h data collection speed. Figure 4(a) shows the exterior of a DHDV equipped with the 3D Ultra technology. With the high power line laser projection system and custom optic filters, DHDV can work at highway speed during day-time and night-time and maintain image quality and consistency. 3D Ultra is the latest imaging sensor technology that is able to acquire both 2D and 3D laser imaging data from pavement surface through two separate left and right sensors (Wang, 2011). The camera and laser working principle is shown in Fig. 4(b). A typical pavement surface in 3D captured at highway speed is shown in Fig. 5 with the cracking analysis result.

Fig. 4 Photographs of (a) DHDV exterior appearance (courtesy of FAA and WayLink); (b) PaveVision 3D working principle.

3.2 Inertial Measurement Unit (IMU)

The Inertial Measurement Unit (IMU) used for 3D Ultra is a self-contained sensor consisting of accelerometers, fibre-optic gyroscopes, and integrated GPS antennas. The physical principle of this type of gyroscope operation is analogous to the Doppler Effect, which involves determination of the phase shift between two counter propagating light beams (Luo et al., 2014). Currently, the IMU has been integrated and synchronized into the DHDV vehicle for geometrical information capture. In this study, the collected IMU data contains GPS coordinates, cross slope, and longitudinal grade, which are utilized for hydroplaning speed prediction.

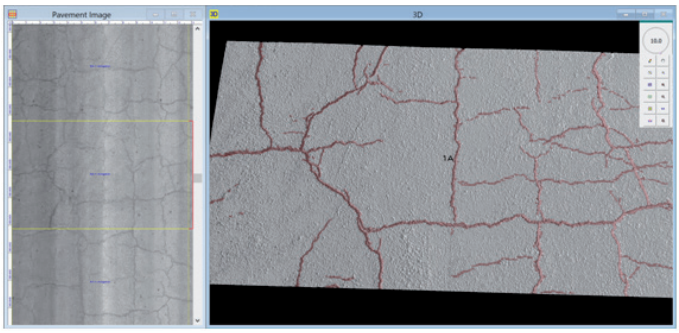

Fig. 5 A Typical 3D (right) and 2D (left) pavement surface captured with 3D Ultra technology at highway speed (courtesy of WayLink)

4 Data Preparation

4.1 Estimated Mean Texture Depth (EMTD)

The methodologies for texture measurements can be grouped into two categories: static and high-speed methods. The static test methods include Sand Patch Method (ASTM, 2006a), Circular Track Meter (ASTM, 2006b), and Outflow Meter (ASTM, 2006c), and their measurements are conducted on the marked or specified small areas. The traditional high-speed test techniques are characterized with the laser-based data acquisition systems (ASTM, 2006d) with a spot laser resulting in a single line of measurement along the longitudinal direction of pavement. The measurements are continuously conducted on test sections, which can be regarded as an efficient tool for network level pavement survey.

The widely used texture indicators include the Mean Profile Depth (MPD) and Mean Texture Depth (MTD) (ASTM, 2006a; ASTM, 2005). In this study, the MTD methodology is applied since the estimation of water film depth is dependent on the MTD in the hydroplaning models. However, as the manual process to obtain MTD through the Sand Patch Method is a standard, time-consuming, and somewhat not reliable enough (Wang, 2014), the 3D pavement surface captured with the 3D Ultra technology is therefore used as an alternative to be used as input to calculate area texture simulating the Sand Patch Method. The alternative substantially improves data collection efficiency and reliability of computing surface texture. As a volumetric method, the Estimated MTD (EMTD) is therefore introduced in the research by simulating the Sand Patch Method with 1mm 3D laser imaging data of the entire lane, as shown in Eq. (13) (Wang and Li, 2011). EMTD and MTD are assumed to be equivalent in the presented research.

$$EMTD = (1/k) \times \sum_{i=1}^{K} \frac{\int_0^D \left[F_0 - F(x,y) \right] dxdy}{D} = (1/k) \times \sum_{i=1}^{K} \frac{\sum_{x=1}^{x=N} \sum_{y=1}^{y=M} \left[F_0 - F(x,y) \right]}{D} \quad (13)$$

Where: $F(x, y)$: The pixel depth at point (x, y); D : The integral or gridded area containing of M×N pixels; F_0 : The maximum peak in each area D; K : The number of grids within the test sample.

4.2 Cross Slope Calibration

A properly designed and constructed cross slope is important for safe travelling since inadequate cross slopes may result in low efficiency in drainage and large cross slopes may lead to vehicle manoeuvring difficulties. Therefore, the accurate measurement of the cross slope is important for hydroplaning speed prediction. In this study, 1mm 3D pavement data and IMU data are combined together to reproduce the cross slope of pavements.

IMU mounted on the vehicle can measure three Euler angles, which are termed as a roll (Euler angle about x-axis), pitch (Euler angle about y-axis) and yaw (Euler angle about z-axis) respectively. The roll angle is to represent pavement cross slope, and the pitch angle is traditionally used to represent pavement longitudinal grade based on the assumption that the vehicle floor is parallel with pavement surface during travelling. However, in real world the vehicle floor is not parallel with pavement surface during travelling, which can be caused by: 1) uneven gravity distribution of the vehicle; 2) vibration of the vehicle during travelling; 3) pavement surface geometry and condition.

This study attempts to measure the vehicle's body roll angle in X coordinate (angle γ) using the collected 3D laser imaging data. Two sensors mounted on the rear of the DHDV are capable of covering the entire lane. The "true" cross slope of pavements can be approximately determined with two parameters: the tilt of the vehicle floor and the slope of pavement surface captured by 3D cameras (Wang et al., 2011). As Figure 6 shows, the IMU system measures the angle θ of the vehicle relative to a level datum. γ is the vehicle vibration angle in X coordinate which can be calculated in Eq. (14). The "true" cross slope can be obtained by Eq. (15). However, in real world the angle and are very small, so the cross slope can be directly computed as the difference in slope of θ and slope of γ (Eq. (16)) (Mekemson et al., 2002).

$$\gamma = act\ \tan\left(\frac{y_2 - y_1}{L}\right) \tag{14}$$

$$\alpha = \tan(\theta + \gamma) \tag{15}$$

$$\alpha = \tan(\theta) + \tan(\gamma) \tag{16}$$

Where: α : Angle of cross slope (degree); γ : The body roll angle of vehicle (degree); θ : IMU roll angle (degree); L : The distance between left and right laser (m); y_1 : The vertical distance from left sensor to the pavement surface (m); y_2 : The vertical distance from right sensor to the pavement surface (m).

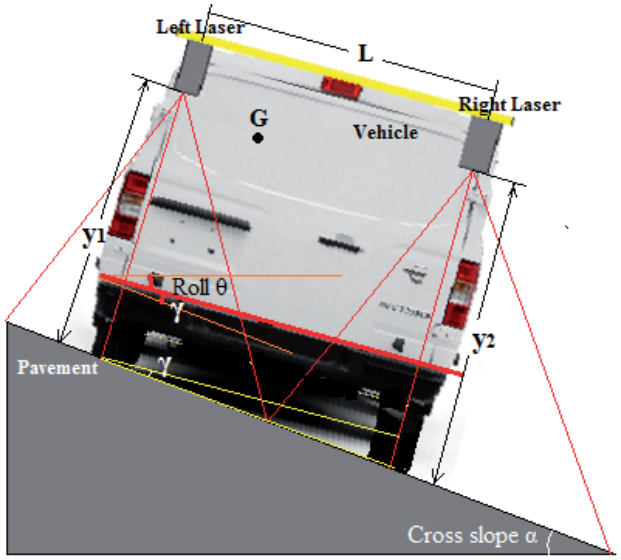

Fig. 6 Cross slope calibration schematic using IMU data and 3D laser imaging data

5 Automated Prediction Program of Hydroplaning

A software program named Automated Hydroplaning Prediction Program (AHPP) is developed in this study to implement data processing and analysis. Figure 7 shows the main interface of AHPP. Once users import the IMU and 3D image data into AHPP, the two types of data (1mm 3D laser imaging data and IMU data) can be automatically matched by Distance Measurement Instrument (DMI) pulses, and the calibrated cross slope can be produced by the integration of IMU data and 3D data. In AHPP, users can manually assign the local rainfall intensity and pavement types. The AHPP outputs include EMTD, WFD, calibrated cross slope, longitudinal grade, and predicted hydroplaning speeds from various models.

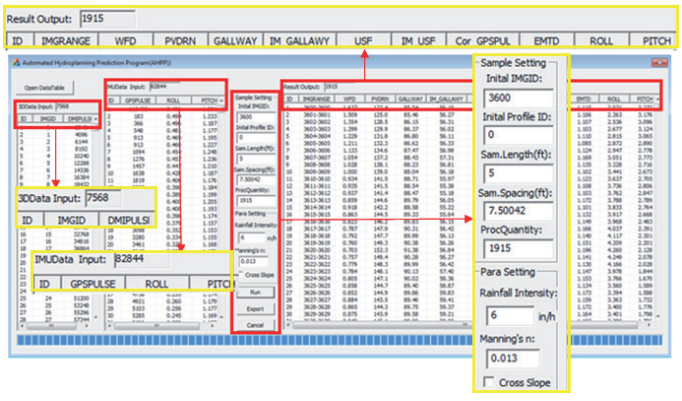

Fig. 7 AHPP operation interface

6 Case Study

6.1 Test Site

A flexible pavement section located in Spavinaw, Oklahoma is chosen as the test section, which starts from the location (Latitude: 36.329175, Longitude: -95.081696), and ends with

the location (Latitude: 36.351066, Longitude: -95.062796), with a length of 4.35 km. The pavement of the test lane is in excellent condition and has a width of 3.65m. On this test section, there are five horizontal curves.

6.2 Selection of Sample Size

The 3D laser imaging data collected with the 3D Ultra DHDV is stored on computer hard disk in the form of raw data files with the size of 4096 pixel wide by 2048 pixel long. The raw data files are used as basic input data sets, or samples and subsequently data processing and analysis are conducted on each individual sample. In this study, one raw image is considered as a sample (2.28m long) and the entire pavement section consists of 1915 samples.

6.3 Local Rainfall Intensity

The local rainfall intensity at the test site is obtained from National Oceanic and Atmospheric Administration's (NOAA) National Water Service database (NOAA, 2014). Table 1 shows the precipitation in Spavinaw Station Oklahoma from NOAA database. The two-year return period storm with duration of five minutes is used in Gallaway and USF models for rainfall intensity acquisition. Based on NOAA database, the rainfall intensity of 148.4mm/hour is used for the test site.

Table 1 Precipitation in Spavinaw Station (23)

Duration (in mm)	Average recurrence interval (years)			
	1	2	5	10
5 min	10.87	12.37	14.91	17.04
10 min	15.93	18.11	21.82	24.97
15 min	19.41	22.09	26.67	30.48
30 min	28.70	32.77	39.62	45.47

6.4 Cross Slope and Longitudinal Grade

Both longitudinal grade and cross slope are the key factors to form flow path slope. As Figure 8(a) shows, the maximum longitudinal grade is 12.03%, and the standard deviation is 2.48. Due to the vibration of the surveying vehicle, there is some noise in the raw cross slope captured by IMU roll angle. Based on the 3D laser imaging data, the vehicle body roll angle can be measured, and then the raw cross slope is calibrated. Figure 8(b) shows the raw cross slope and calibrated cross slopes. Comparing the raw cross slope data and calibrated cross slope, the majority of the noise is eliminated from the raw data through the calibration. The cross slope presents negative values at left turn curves and positive values at right turn curves. In this test site, curves #1, #4, and #5 belong to left turn curve, while curves #2 and #3 belong to right turn curve. The statistical results of the calibrated cross slopes on test site are given as follows: (1) the average cross slope on the straight road segments is 1.94%; (2) the average cross slope of curve #1, #2, #3, #4, and #5 are -2.06%, 4.96%, 5.80%, -3.81%, and -5.01%, respectively.

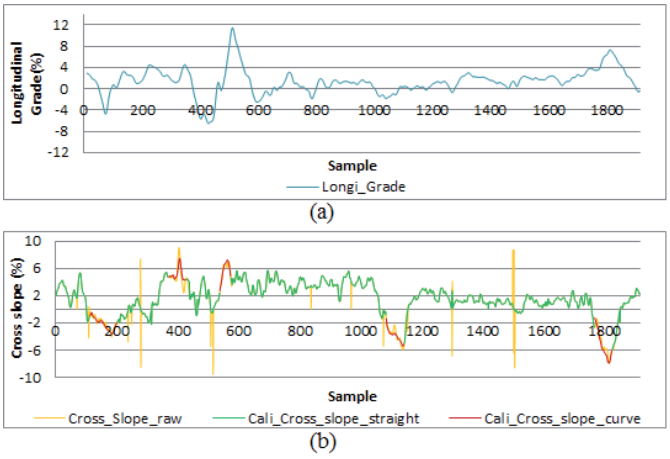

Fig. 8 Pavement geometry of test site: (a) Longitudinal grade; (b) Cross slope.

6.5 EMTDs and WFDs

Figure 9(b) shows the EMTDs at the test section, with an average value of 1.20 mm, and Fig. 9(a) shows the corresponding WFD along the test section, with an average value of 1.73mm and the maximum value of 8.52 mm. The WFD is calculated with Gallaway WFD model based on pavement texture depth, flow path slope, and local rainfall intensity as inputs.

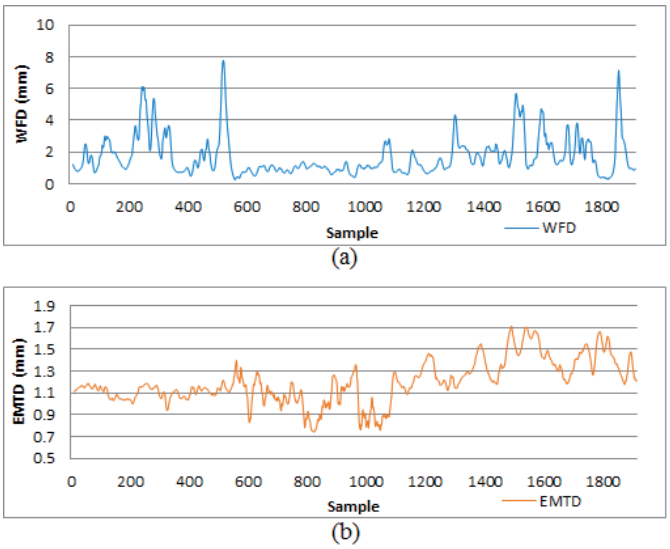

Fig. 9 WFDs and EMTDs of test site: (a) WFDs; (b) EMTDS.

6.6 Hydroplaning Speed Estimation

13 samples of the calculated WFD, EMTD and IMU data for hydroplaning speed prediction are given in Table 2. Gallaway model, USF model, the improved Gallaway model, and the improved USF model are utilized to predict hydroplaning speed, respectively, as shown in Figure 10(a). Results indicate the predicted hydroplaning speeds from original Gallaway and USF model are approximately 140km/h and 165km/h, respectively, which are around 50km/h higher than those predicted

from the improved Gallaway model (96km/h) and improved USF model (91km/h). The results also show as expected that the hydroplaning speeds at curves of the five horizontal curves in Fig. 10(a) are lower than that on the straight road sections.

Table 2 Samples of 3D Imaging Data and IMU Data for Hydroplaning Speed Calculation

Sample ID	WFD (mm)	EMTD (mm)	Cross Slope (%)	Longitudinal Grade (%)
1	1.64	1.12	2.07	3.27
2	1.51	1.11	2.26	3.18
3	1.35	1.11	2.54	3.10
4	1.30	1.10	2.68	3.12
5	1.23	1.11	2.82	3.07
6	1.21	1.09	2.87	2.89
7	1.13	1.12	2.95	2.78
8	1.05	1.17	3.05	2.77
9	1.03	1.14	3.23	2.72
10	1.00	1.10	3.44	2.67
11	0.93	1.12	3.64	2.71
12	0.94	1.11	3.74	2.81
13	0.94	1.10	3.76	2.85
14	0.86	1.17	3.79	2.79
15	0.92	1.10	3.83	2.76

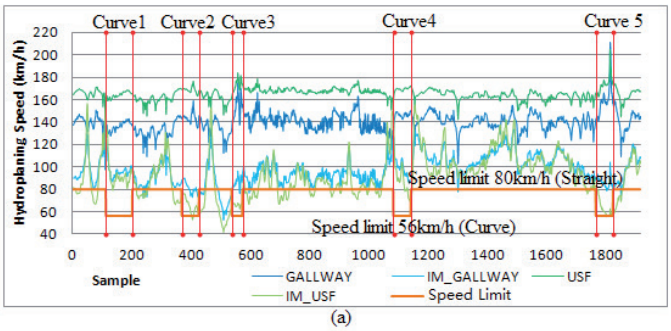

(a)

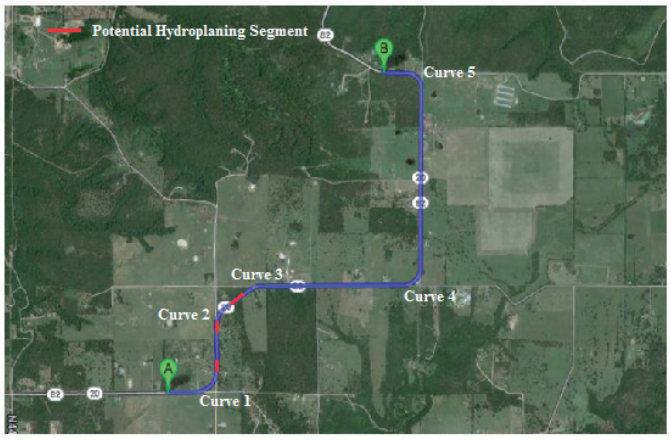

(b)

Fig. 10 Potential hydroplaning detection: (a) hydroplaning speed; (b) hydroplaning hazardous segments.

6.7 Potential Hydroplaning Segment Detection

Identification of hazardous locations with hydroplaning potential is based on the comparison of estimated hydroplaning speed with posted speed of the road section (Luo et al., 2014). At the test site, speed limits are 80km/h on straight sections and 56km/h on road curves. The average hydroplaning speeds calculated with the four models are used to detect potential hydroplaning segments, shown in Fig. 10(a). Since the predicted hydroplaning speeds at the five curves are higher than posted speed limit, there is a low hydroplaning risk at the five curves for vehicles operating at the speed limit. However, for several segments of the test site, the predicted hydroplaning speeds are lower than the posted speed limit. Therefore, these segments can be identified as potential hazardous segments for hydroplaning risk, as marked with the red line in Figure 10(b). To minimize traffic accidents caused by hydroplaning, highway agencies can post a reduced speed sign at these locations, or take other remedial actions, such as installing High-Friction Surface Treatment (HFST) (Shah and Jain, 2014).

7 Conclusions

To take into account the effects of flow path slope on vertical wheel load perpendicular to pavement surface and the resulting hydroplaning speed, the Gallaway and USF models are modified for improvements in this study. The sensitivity analysis shows that the hydroplaning speed is more sensitive to cross slope than longitudinal grade in the improved models. A volumetric measuring method is used to calculate Estimated MTD based on the entire lane data. IMU data and 3D laser imaging data are combined together to realistically model vehicle movements on cross slopes. Local rainfall intensity is obtained from NOAA precipitation database. By considering effects of cross slope and longitudinal grade on wheel load and flow path length, it is found that hydroplaning speed decrease with the increase of the longitudinal grade, but increase with the increase of the cross slope. The improved models provided lower hydroplaning speed than original Gallaway and USF models. An important future work is to use a combined slope based on longitudinal grade and cross slope to demonstrate the validity and effectiveness of the improved models.

References

ASTM (2005) Standard Practice for Calculating Pavement Macrotexture Mean Profile Depth. ASTM Standard Practice E 1845-01. *Book of ASTM Standards, Volume 04.03.* Philadelphia.

ASTM (2006a) Measuring Pavement Macrotexture Depth Using a Volumetric Technique. ASTM Standard Practice E 965. *Book of ASTM Standards. Volume 04.03.* Philadelphia.

ASTM (2006b) Measuring Pavement Macrotexture Properties Using the Circular Track Meter. ASTM Standard Practice E 2157. *Book of ASTM Standards. Volume 04.03.* Philadelphia.

ASTM (2006c) Measuring Pavement Texture Drainage Using an Outflow. ASTM Standard Practice E 2380. *Book of ASTM Standards. Volume 04.03.* Philadelphia.

ASTM (2006d) Measuring Surface Frictional Properties Using the British Pendulum Tester. ASTM Standard Practice E 303. *Book of ASTM Standards. Volume 04.03.* Philadelphia.

Berta, T, Torok, A. (2009) Changes In Road Safety Tendecies Due To Climate Change In Hungary. In: *Proceedings of the International Scientific Conference Modern Safety Technologies in Transportation 2009.* 22-24 September 2009. Zlata Idka. pp. 27-30.

Chesterton, J., Nancekivell, N., Tunnicliffe, N. (2006) The use of the Gallaway Formula for Aquaplaning Evaluation in New Zealand. *Transit New Zealand and New Zealand Institute of Highway Technology (NZIHT) 8th Annual Conference.*

Dabbour, E. (2012) Using logistic regression to identify risk factors causing rollover collisions."*International Journal of Traffic and Transport Engineering*. 2(4). pp. 372-379. DOI: 10.7708/ijtte.2012.2(4).07

Dzerkelis, V., Bazaras, Ž., Lukoševičius, V. (2015) Investigation of the influence of A-pillar on passive safety of a vehicle in case of rollover. *Transport*. 30 (2). pp. 194-201. DOI: 10.3846/16484142.2015.1045937

Gallaway, B. M., et al. (1979) Pavement and Geometric Design Criteria for Minimizing Hydroplaning. Federal Highway Administration. Report No. FHWA-RD-79-31

Gallaway, B. M., Rose, G. (1971) The Effects of Rainfall Intensity, Pavement Cross Slope, Surface Texture, and Drainage Length on Pavement Water Depths."Texas Transportation Institute, Research Report No. 138-5

Goyal, R. (2003) Design and Analysis of Interceptor Drains—Effect of Parameters. *ISH Journal of Hydraulic Engineering*. 9 (1). pp. 61-71. DOI: 10.1080/09715010.2003.10514721

Gunaratne, M., Lu, Q., Yang, J. (2012) Hydroplaning on Multi Lane Facilities. Report for Florida Department of Transportation, Report No. BDK84 977-14, 2012.

Horne, W.B., Dreher, R. C. (1963) Phenomena of Pneumatic Tire Hydroplaning. NASA TN D-2-56, NASA Langley Research center, NASA, Hampton, VA.

Huebner. R. S., Anderson, D., Warner, J., Reed, J.(1996) PAVDRN Computer Model for Predicting Water Film Thickness and Potential or Hydroplaning on New and Reconditioned Pavements. *Transportation Research Record: Journal of the Transportation Research Board.* 1599. pp. 128-131. DOI: 10.3141/1599-16

Khedr, S. A., Breakah, T. M. (2011) Rutting parameters for asphalt concrete for different aggregate structures. *International Journal of Pavement Engineering*. 12 (1). pp. 13-23. DOI: 10.1080/10298430903578960

Kumar, S. S., Kumar, A., Fwa, T. F. (2009) Analyzing effect of tire groove patterns on hydroplaning speed. *Journal of the Eastern Asia Society for Transportation Studies*. 8.

Luo, W., Wang, K. C. P., LiL (2014) Surface Drainage Evaluation for Rigid Pavements Using IMU and 1 mm 3D Texture Data. *Transportation Research Record: Journal of the Transportation Research Board*. pp. 121–128.

Mekemson et al. (2002) Method and Apparatus for Pavement Cross-slope Measurement, Patent Application Publication, Pub. No.: US 2002/0013644 A1

NOAA's National Water Service (2014) Hydrometeorological Design Studies Center. [Online] Precipitation Frequency Data Server (PFDS) Available from: http://dipper.nws.noaa.gov/hdsc/pfds/ [Accessed: 21th July 2014]

Ong, G. P., Fwa, T. F. (2007) Wet-pavement hydroplaning risk and skid-resistance: Modeling. *ASCE Journal of Transportation Engineering.* 133 (10). pp. 590-598. DOI: 10.1061/(ASCE)0733-947X(2007)133:10(590)

Russam, K., Ross, N. F. (1968) The Depth of Rain Water on Road Surfaces. Road Research Laboratory. *Ministry of Transport Report* No. LR 236, pp. 25.

Shafabakhsh, G. A., Kashi, E. (2015) Effect of Aircraft Wheel Load and Configuration on Runway Damages. *Periodica Polytechnica Civil Engineering.* 59 (1). pp. 85-94. DOI: 10.3311/PPci.2103

Vujanic, M., Lipovac, K., Jovanovic, D., Pesic, D., Antic, B. (2013) "Bottom-Up" and "Top-Down". Approach for Defining Road Safety Strategy-Case Study: City of Belgrade. *International Journal for Traffic and Transport Engineering*. 3 (2). pp. 185-203. DOI: 10.7708/ijtte.2013.3(2).07.

Wang, K. C. P., Li, L. (2011) Potential Measurement of Pavement Surface Texture based on Three-Dimensional (3D) Image Data. *Transportation Research Board 91th Annual Meeting*. Washington.

Wang, K. C. P., Luo, W., Li, J. Q. (2014). Hydroplaning Risk Evaluation of Highway Pavements based on IMU and 1 mm 3D Texture Data. *T&DI Congress 2014: Planes Trains, and Automobiles*, Advanced Technologies for Transportation Application. pp. 511-522.

Wang, K. C. P. (2011) Automated Survey of Pavement Distress based on 2D and 3D Laser Images. *Report for MBTC* DOT 3023, 2011.

Wang, K. C. P. (2014) Safety Evaluation of Pavement Surface Characteristics with 1mm 3D Laser Imaging. RiP Project 37465, Nov 7 2014.

Yogesh U. S., Jain, S. S., Manoranjan, P. (2014) Evaluation of prioritization methods for effective pavement maintenance of urban roads. *International Journal of Pavement Engineering*. 15 (3). pp. 238-250. DOI: 10.1080/10298436.2012.657798

Zhang, Z., Abu-Farsakh, M. Y., Tao, M. (2005) Evaluation of trench backfills at highway cross-drains. *International Journal of Pavement Engineering*. 6 (2). pp. 77-87. DOI: 10.1080/10298430500137228